



Physiologically based kinetic modeling of hesperidin metabolism and its use  
to predict in vivo effective doses in humans

Boonpawa, R., Spenkeliink, B., Punt, A., & Rietjens, I.

This article is made publically available in the institutional repository of Wageningen University and Research, under article 25fa of the Dutch Copyright Act, also known as the Amendment Taverne.

Article 25fa states that the author of a short scientific work funded either wholly or partially by Dutch public funds is entitled to make that work publicly available for no consideration following a reasonable period of time after the work was first published, provided that clear reference is made to the source of the first publication of the work.

For questions regarding the public availability of this article, please contact [openscience.library@wur.nl](mailto:openscience.library@wur.nl).

Please cite this publication as follows:

Boonpawa, R., Spenkeliink, B., Punt, A., & Rietjens, I. (2017). Physiologically based kinetic modeling of hesperidin metabolism and its use to predict in vivo effective doses in humans. *Molecular Nutrition & Food Research*, 61(8), [1600894]. <https://doi.org/10.1002/mnfr.201600894>

## RESEARCH ARTICLE

# Physiologically based kinetic modeling of hesperidin metabolism and its use to predict in vivo effective doses in humans

Rungnapa Boonpawa, Albertus Spenkelink, Ans Punt\* and Ivonne M. C. M. Rietjens

Division of Toxicology, Wageningen University & Research, Wageningen, The Netherlands

**Scope:** To develop a physiologically based kinetic (PBK) model that describes the absorption, distribution, metabolism, and excretion of hesperidin in humans, enabling the translation of in vitro concentration–response curves to in vivo dose–response curves.

**Methods and results:** The PBK model for hesperidin in humans was developed based on in vitro metabolic parameters. Hesperidin was predicted to mainly occur in the systemic circulation as different monoglucuronides. The plasma concentrations of hesperidin aglycone (hesperetin) was predicted to be <0.02 mg/L at an oral dose of 50 mg/kg bw. The developed PBK model allowed conversion of in vitro concentration–response curves for different effects to in vivo dose–response curves. The BMD<sub>05</sub> (benchmark dose for 5% response) values for protein kinase A inhibition ranged between 135 and 529 mg/kg bw hesperidin, and for inhibition of endothelial cell migration and prostaglandin E<sub>2</sub> and nitric oxide production ranged between 2.19 and 44 mg/kg bw hesperidin. These values are in line with reported human data showing in vivo effects by hesperidin and show that these effects may occur at Western dietary and supplementary intake of hesperidin.

**Conclusions:** The developed PBK model adequately predicts absorption, distribution, metabolism, and excretion of hesperidin in humans and allows to evaluate the human in vivo situation without the need for human intervention studies.

## Keywords:

ADME / Hesperetin metabolites / Hesperidin / In vitro–in vivo extrapolation / PBK modeling



Additional supporting information may be found in the online version of this article at the publisher's web-site

## 1 Introduction

Hesperidin (hesperetin-7-O-rutinoside) is the  $\beta$ -glycoside form of the flavanone hesperetin, and is almost exclusively

present in citrus fruits, especially in orange [1]. Sweet orange juice contains 487–584 mg hesperidin/L [2]. Hesperidin and its aglycone, hesperetin, have been suggested to exert various beneficial health effects against many degenerative diseases including cancer, cardiovascular diseases, osteoporosis, obesity, and diabetes [3–5]. In addition also beneficial health effects have been reported for hesperetin metabolites based on their interaction with various key proteins such as protein kinases [6–9] and via induction or reduction of specific genes related to cellular functions [10–12]. During uptake following oral ingestion, hesperidin and its aglycone hesperetin are extensively metabolized in intestinal and liver tissue and as a result hesperetin is mostly present in the systemic circulation in conjugated forms [13–16]. This raises the question

**Correspondence:** Dr. Rungnapa Boonpawa

**E-mail:** boonpawa\_5@hotmail.com

**Abbreviations:** ADME, absorption, distribution, metabolism, and excretion; C<sub>max</sub>, maximum concentration; EC<sub>in vitro</sub> or *in vivo*, effective *in vitro* or *in vivo* concentration; GI, gastrointestinal; H-7G, hesperetin-7-O-glucuronide; H-3'G, hesperetin-3'-O-glucuronide; H-3'S, hesperetin-3'-O-sulfate; H-3'7diG, hesperetin-3',7-O-diglucuronide; H-7G-3'S, hesperetin-7-O-glucuronide-3'-O-sulfate; NO, nitric oxide; PAPS, 3'-phosphoadenosine 5'-phosphosulfate; PBK, physiologically based kinetic; PGE<sub>2</sub>, prostaglandin E<sub>2</sub>; PKA, protein kinase A; SC, sensitivity coefficient; UDPGA, uridine 5'-diphosphoglucuronide acid

\*Current address: Ans Punt, RIKILT—Wageningen University & Research Wageningen, The Netherlands.

Received: October 11, 2016

Revised: January 31, 2017

Accepted: February 13, 2017

of whether any in vivo biological effect of hesperidin or hesperetin is due to the free aglycone hesperetin or perhaps, at least in part, to these metabolites. Little is known about physiologically relevant concentrations of hesperetin aglycone and its circulating metabolites in vivo. For a better translation of in vitro results to in vivo effects, it is of importance to gain more insight in absorption, distribution, metabolism, and excretion (ADME) of hesperidin upon ingestion, especially to obtain an indication of the physiologically relevant plasma concentrations of hesperetin aglycone and its circulating metabolites.

Dietary intake of hesperidin in Western countries is estimated to be 193–562 mg hesperidin corresponding to 2.8–8 mg/kg bw for a 70 kg person [17]. Hesperidin is also available as a food supplement with daily doses of 500–2000 mg hesperidin corresponding to 7–29 mg/kg bw for a 70 kg person [18]. Figure 1 illustrates the proposed metabolic pathways of dietary hesperidin in humans. Upon oral ingestion, hesperidin cannot be hydrolyzed by  $\beta$ -glucosidases in the small intestine, but passes to the colon, where it can be hydrolyzed to hesperetin aglycone by colonic microbiota prior to its absorption into the colonic enterocyte [14]. The release of hesperetin is the rate-limited step for absorption [16]. In contrast to hesperidin, hesperetin aglycone can be directly taken up in the small intestinal enterocyte by passive diffusion [14]. The absorbed hesperetin is metabolized by UDP-glucuronosyl transferases and sulfotransferases in the colon, small intestine, and liver at the 3'- and 7-position [19]. Several metabolites of hesperetin including mono- and diconjugates have been identified in human urine, indicating further conjugation of monoconjugates [13, 15, 20].

To better understand in vivo effects of dietary hesperidin, the present study aimed to develop a physiologically based kinetic (PBK) model for hesperidin to gain insight in dose-dependent plasma concentrations of hesperetin aglycone and its metabolites. The developed PBK model was subse-

quently combined with in vitro effect data using a so-called reverse dosimetry approach to determine whether in vitro effects of hesperetin and its metabolites can also be expected to occur in vivo, and if so, at what hesperidin oral dose levels.

## 2 Materials and methods

### 2.1 Materials

Pooled mixed-gender human tissue fractions including small intestine microsomes, small intestine cytosol, liver microsomes, liver cytosol, and individual male colon S9 were purchased from Xenotech (Lenexa, USA). Uridine 5'-diphosphoglucuronide acid (UDPGA, purity 98%), 3'-phosphoadenosine 5'-phosphosulfate (PAPS, purity 65%), Tris, alamethicin (from *Trichoderma viride*), D-saccharic acid 1,4-lactone monohydrate, and DTT were purchased from Sigma-Aldrich (Steinheim, Germany). Hydrochloric acid (fuming 37%), magnesium chloride, TFA (for spectroscopy), potassium dihydrogen phosphate, dipotassium hydrogen phosphate trihydrate, and DMSO were purchased from VWR International (Darmstadt, Germany). ACN (chromatography grade) was purchased from Biosolve (Valkenswaard, The Netherlands). Hesperetin (>99%) was purchased from Extrasynthese (Genay Cedex, France). Hesperetin-7-O-glucuronide (H-7G) was purchased from Toronto Research Chemicals (Toronto, Canada). Hesperetin-3'-O-glucuronide (H-3'G) and hesperetin-3',7-O-diglucuronide (H-3'7diG) were purchased from Apollo Scientific (Cheshire, UK). Recombinant human cAMP-dependent protein kinase, catalytic subunit  $\alpha$  (PKA- $\alpha$ ), kemptide (LRRASLG), ATP, and staurosporine were purchased from Biaffin (Kassel, Germany). ADP was purchased from DiscoverRx (Birmingham, UK).

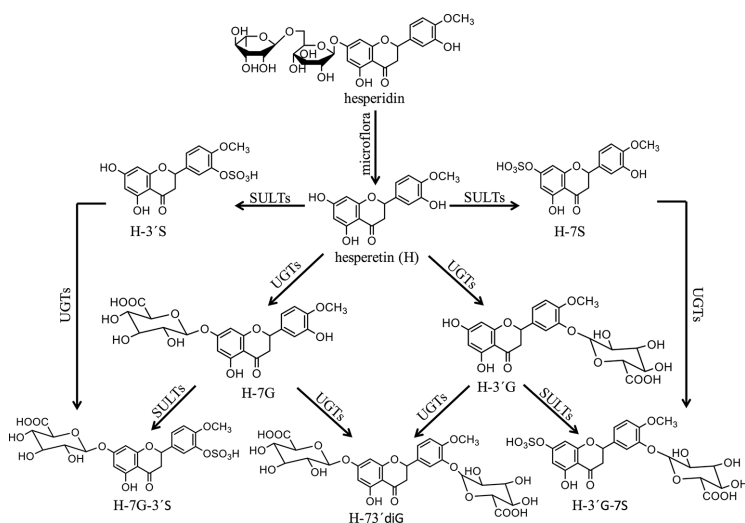


**Figure 1.** Proposed metabolic pathways of dietary hesperidin and hesperetin in humans: glucuronide (G) and sulfate (S) [13, 15, 20].

## 2.2 Enzymatic conjugation of H-7G and H-3'G with pooled human tissue fractions

To obtain kinetic parameters for glucuronidation and sulfation of the monoconjugates, H-7G and H-3'G, to diconjugates, *in vitro* incubations with human tissue fractions were performed according to the methods described by Brand et al. [19] with some modifications. For glucuronidation, 100  $\mu$ L incubation mixtures were prepared containing (final concentrations) 10 mM MgCl<sub>2</sub>, 10 mM UDPGA, 0.025 mg/mL alame-thicin (added from a 200 times concentrated stock solution in methanol), and human tissue fractions in 50 mM Tris-HCl (pH 7.4). For incubations with H-7G, a protein content of 0.6 mg/mL small intestine microsomes, 0.6 mg/mL liver microsomes, or 0.8 mg/mL colon S9 and incubation times of 4, 2, or 6 h were applied. For incubations with H-3'G, a protein content of 0.3 mg/mL small intestine microsomes, 1.0 mg/mL liver microsomes, or 0.8 mg/mL colon S9 and incubation times of 4, 3, or 6 h were applied. The reactions were initiated by adding H-7G or H-3'G from 200 times stock solutions in DMSO (final concentration of the substrate ranging from 5 to 400  $\mu$ M) and were terminated by adding 25  $\mu$ L of ice-cold ACN. Blank incubations were carried out without UDPGA. Under the specified conditions, glucuronidation was linear with time and protein content (data not shown).

For sulfation, 100  $\mu$ L incubation mixtures were prepared containing (final concentrations) 5 mM MgCl<sub>2</sub>, 0.1 mM PAPS, 20 mM saccharic acid-1,4-lactone (pH 7.4) as  $\beta$ -glucuronidase inhibitor [21], and human tissue fractions in 50 mM potassium phosphate (pH 7.4). For incubations with H-7G, a protein content of 0.8 mg/mL small intestine cytosol, liver cytosol, or colon S9 and incubation times of 3, 4, or 6 h were applied. For incubations with H-3'G, a protein content of 0.8 mg/mL small intestine cytosol, liver cytosol, or colon S9 and incubation times of 5, 4, or 6 h were applied. The reactions were initiated by adding H-7G or H-3'G from 200 times stock solutions in DMSO (final concentration of the substrate ranging from 5 to 400  $\mu$ M) and were terminated by adding 25  $\mu$ L of ice-cold ACN. Blank incubations were carried out without PAPS. Under the specified conditions, sulfation was linear with time and protein content (data not shown).

## 2.3 Identification and quantification of hesperetin metabolites

All incubation samples were analyzed on a UPLC-DAD system consisting of a Waters (Milford, MA) Acquity binary solvent manager, sample manager, and photodiode array detector, equipped with a Waters Acquity UPLC BEH C18 column (1.7  $\mu$ m, 2.1  $\times$  50 mm) at 40°C column temperature. All samples were centrifuged at 15 000 rpm for 5 min at 5°C to precipitate proteins and 3.5  $\mu$ L of the supernatant was subsequently analyzed using the UPLC-DAD system. A gradient was applied consisting of nanopure water containing 0.1% TFA (eluent A) and acetonitrile (eluent B) with a flow rate of

0.6 mL/min with the following profile: 0–25% B (0–1.0 min), 25% B (1.0–3.0 min), 25–50% B (3.0–4.0 min), 50–80% B (4.0–4.5 min), 80% B (4.5–5.5 min), 80–0% B (5.5–6.0 min), and 0% B (6.0–8.0 min).

The diglucuronide, H-3'7diG, formed by glucuronidation of either H-7G or H-3'G was identified by comparing its UV spectrum and retention time with those of commercially available H-3'7diG. The nature of the sulfate metabolite of H-7G and H-3'G was confirmed by treating the un-terminated incubation samples with  $\beta$ -glucuronidase/sulfatase as there was no commercially reference compound available. To this end, 50  $\mu$ L of un-terminated incubation samples were added to 50  $\mu$ L of 0.1 M sodium acetate (pH 5.0) containing 189 units/mL  $\beta$ -glucuronidase and 1 unit/mL sulfatase. The reactions were carried out for 3 h at 37°C and were terminated by adding 25  $\mu$ L of ice-cold acetonitrile.

All formed metabolites were quantified by integrating the peak area at 280 nm and by using a calibration curve of H-3'7diG. The sulfate metabolites of H-7G and H-3'G were quantified based on the calibration curve of H-3'7diG, which was considered adequate because the sulfate metabolites of H-7G and H-3'G appeared to have the same UV-spectrum as H-3'7diG (Supporting Information) and were assumed to display a similar molar extinction coefficient.

The kinetic parameters including the apparent maximum velocity ( $V_{\max(\text{app})}$ ) and apparent Michaelis–Menten constant ( $K_{\text{m}(\text{app})}$ ) for different conjugation reactions were determined by fitting the data to the standard Michaelis–Menten equation with GraphPad Prism version 5.04 (GraphPad Software, San Diego, CA, USA). The Michaelis–Menten equation was as follows:

$$v = V_{\max} * [S] / (K_m + [S]) \quad (1)$$

where [S] represents the substrate concentration. The values of  $V_{\max}$  and  $K_m$  were expressed in nmol/min/mg protein and  $\mu$ M, respectively.

## 2.4 Protein kinase A inhibition assay

A protein kinase A (PKA) inhibition assay was carried to measure the potency of hesperetin and its monoglucuronides H-7G and H-3'G to inhibit PKA as possible mechanism underlying some of its beneficial effects [22,23]. The PKA inhibition assay was carried out based on the method described by Chen et al. [24] with some modifications. The incubation mixtures (final volume 50  $\mu$ L) contained (final concentrations) 5 mM MgCl<sub>2</sub>, 0.5 mM DTT, 96 ng/mL PKA, 4  $\mu$ M kemptide (PKA substrate), hesperetin, H-7G, or H-3'G added from a 100 times concentrated stock in DMSO (final concentration ranging from 0 to 500  $\mu$ M) in 50 mM Tris-HCl (pH 7.4). The final concentration of DMSO was kept at 1% for all incubations. The positive control for PKA inhibition was carried out using 10  $\mu$ M staurosporine (final concentration), a potent protein kinase inhibitor with a reported IC<sub>50</sub> value of

0.015  $\mu\text{M}$  [25]. The concentration of the substrate kemptide was selected to be close to the  $K_m$  value of 4.3  $\mu\text{M}$  at 5  $\mu\text{M}$  ATP for ADP induction (data not shown). The incubation mixtures were preincubated for 3 min at 30°C prior to initiation of the reactions by adding 5  $\mu\text{M}$  ATP (final concentration). After 30 min, the reactions were terminated by adding 50  $\mu\text{L}$  of ice-cold ACN. Under the specified conditions, ADP formation was linear with time and protein content (data not shown).

All samples were centrifuged at 15 000 rpm for 5 min at 5°C to precipitate proteins and 5  $\mu\text{L}$  of the supernatants were subsequently analyzed on a UPLC-DAD system consisting of a Waters (Milford, MA) Acquity binary solvent manager, sample manager, and photodiode array detector, equipped with a Waters Acquity UPLC BEH Amide column (1.7  $\mu\text{m}$ , 2.1  $\times$  100 mm) at 30°C column temperature. ADP, a by-product from the phosphorylation reactions, was measured at isocratic conditions (70:30–acetonitrile:27 mM  $\text{KH}_2\text{PO}_4$  in nanopure water pH 4.5) for 8 min and at a flow rate of 0.5 mL/min. With this method, ADP eluted at 2.02 min based on the retention time and UV spectrum of commercially available ADP. Triplicate experiments were performed. The inhibitory potency of hesperetin and its monoglucuronides was determined based on comparison to the kinase activity in a blank incubation performed without added inhibitor containing 1% DMSO. The obtained concentration–response curves were translated to in vivo dose–response curve (Section 2.6)

## 2.5 PBK model

A PBK model for dietary hesperidin was developed in a similar manner as previously described for the development of a PBK model for quercetin [26, 27]. The PBK model was defined to gain more insight in the ADME characteristics of hesperidin and the various metabolites formed in humans and to provide a method for conversion of in vitro effective concentrations to in vivo dose levels (Section 2.6). The model consisted of separate compartments for gastrointestinal (GI) tract lumen, small intestine, colon, liver, kidney, rapidly perfused tissues (e.g. heart, lung, brain), and slowly perfused tissues (e.g. skin, muscle, bone) as shown in Fig. 2A and B for the mono- and diconjugates of hesperetin. Hesperidin was modeled to be hydrolyzed to its aglycone, hesperetin, by microbiota in the colon prior to absorption. The rate constants for hydrolytic clearance of hesperidin by the colonic microbiota, for excretion via urine or bile, and for the intestinal efflux back to the intestinal lumen were obtained by fitting with available experimental human data [13, 15, 16, 28–30], resulting in values of 0.1 L/h, 30  $\text{h}^{-1}$ , 30  $\text{h}^{-1}$ , and 0.2 L/h, respectively. The hesperetin that is released within the lumen was modeled to be absorbed into the colonic enterocyte by passive diffusion. The absorption rate constant for intestinal uptake of hesperetin is not available. An in situ intestinal perfusion study showed that the rate transfer of hesperetin to the intestinal wall was similar to that for genistein [31]. Based on this observation, the absorption rate constant of hesperetin

was assumed to be similar to that for genistein with a value of 5  $\text{h}^{-1}$  [32]. To take the transit time of hesperidin from the stomach to the colon into account, the GI transit rates were included using the values reported by Kimura et al. [33] of 4.63, 2.44, and 2.76  $\text{h}^{-1}$  for stomach, jejunum, and ileum, respectively.

Hesperetin was modeled to primarily converse via glucuronidation and sulfation forming four different monoconjugates at the 3'- and 7-position in small intestine, colon, and liver. Further conjugation of different monoconjugates to diconjugates was simulated only for the mono-glucuronides, H-7G and H-3'G, since these metabolites were estimated to be the major primary metabolites formed accounting for approximately 70% of the hesperidin dose based on model stimulation (data not shown). The kinetic constants for formation of monoconjugates of hesperetin in small intestine, colon, and liver were taken from the study of Brand et al. [19] (Section 3.2). The kinetic constants for further conjugations of H-7G and H-3'G via glucuronidation and sulfation were obtained in the present study from in vitro incubations with relevant human tissue fractions (Section 3.1–3.2). The  $V_{\text{max}}$  values for formation of different mono- and diconjugates were scaled to in vivo  $V_{\text{max}}$  values using a small intestine protein yield of 20.6 mg microsomal protein and 18 mg cytosolic protein [34] and a liver protein yield of 40 mg microsomal protein and 80.7 mg cytosolic protein [35]. The scaling factors for colonic metabolism were calculated based on the methods described by van de Kerkhof et al. [36] using the reported data that the colonic tissue of male F344 rat with 24 mg wet weight contained 3 mg protein [37]. A microsomal protein yield of 2.4 mg and a cytosol protein yield of 16.4 mg were calculated and used as scaling factors for colonic metabolism.

The physiological parameters for humans were obtained from literature [38] and are shown in Table 1 in the Supporting Information. The tissue:blood partition coefficients of hesperetin and its metabolites were estimated from log  $K_{\text{ow}}$  according to the method described by DeJongh et al. [39] and are shown in Table 2 in the Supporting Information. Log  $K_{\text{ow}}$  values were estimated from Clog  $P$  values obtained from Scifinder (American Chemical Society, USA) and ChemBio-Draw Ultra 14.0 (Cambridge-Soft, USA). Conversion of blood concentrations of hesperetin and its metabolites to plasma concentrations was done by dividing the blood concentrations by a blood/plasma ratio ( $R$ ). This value was calculated using the Simcyp prediction tool [40, 41] and amounted to 0.66. Mass balance equations were numerically integrated in Berkeley Madonna version 8.3.18 (Macey and Oster, UC Berkeley, CA) using Rosenbrock's algorithm for stiff system. Mass balance equations for hesperetin and its metabolites were similar to those previously described by Boonpawa et al. [26, 27] for PBK models of quercetin. Model performance was evaluated by comparing the predicted concentrations of urinary profiles to reported data in human urine [1, 13, 42]. Further evaluation was done by performing a sensitivity analysis to assess key parameters that contribute substantially to the maximum concentration ( $C_{\text{max}}$ ) of hesperetin aglycone

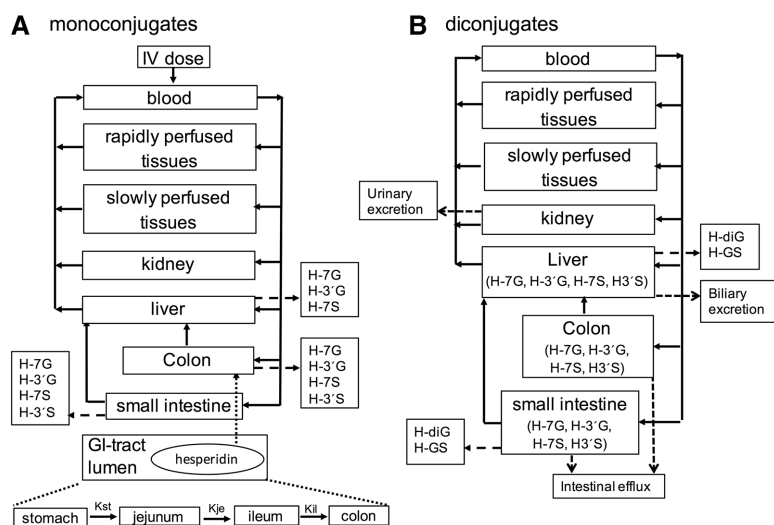


**Figure 2.** PBK model structure for formation of (A) mono- and (B) diconjugates of hesperetin:  $K_{Ti}$  = transit rate constant for stomach (st), jejunum (je), and ileum (il), hesperetin-7-O-glucuronide (H-7G), hesperetin-3'-O-glucuronide (H-3'G), hesperetin-7-O-sulfate (H-7S), hesperetin-3'-O-sulfate (H-3'S), hesperetin-3',7-O-diglucuronide (H-diG), and hesperetin-O-monoglucuronide-O-monosulfate (H-GS).

and its metabolites in plasma at an oral dose of 2.8 and 29 mg/kg bw hesperidin representing the lowest and the highest hesperidin intake from Western diet and food supplements [17, 18]. Normalized sensitivity coefficients (SCs) were calculated for the model parameters according to the method described by Evens and Andersen as follows [43]:

$$SC = (C' - C) / (P' - P) \times (P/C) \quad (2)$$

where  $C$  is the initial value of the model output,  $C'$  is the modified value of the model output resulting from an increase in parameter value,  $P$  is the initial parameter value and  $P'$  is the modified parameter value, taking a 5% increase in its value.

## 2.6 Translation of in vitro effect concentrations to in vivo dose levels

PBK-based reverse dosimetry was carried out to convert *in vitro* effect concentrations to predicted *in vivo* dose levels of hesperidin based on the methods described by Louisse et al. [44] and Strikwold et al. [45]. To this end, biological effects of hesperetin and its metabolites derived from *in vitro* bioassays were used including inhibition of PKA activity by hesperetin and its monoglucuronides (Section 3.5) and available *in vitro* literature data for biological effects of hesperetin and its monoconjugates on inhibition of cell migration induced by TNF- $\alpha$  in human aortic endothelial cells [46] and inhibition by hesperetin metabolite mixtures (mainly monoconjugates) on prostaglandin  $E_2$  (PGE $_2$ ) and nitric oxide (NO) production induced by LPS in RAW 264.7 cells [9]. These *in vitro* data also showed that not only hesperetin aglycone, but also its metabolites could exert similar biological effects with comparable potency, indicating that *in vivo* effects of hesperidin may be due to a mixture of hesperetin aglycone and its metabolites rather than an individual compound. Therefore, the *in vitro* effect concentrations obtained for hesperetin and its

metabolites for the respective effects were added up to obtain the *in vitro* mixture effect concentrations by using the concept of concentration addition as follows [47]:

$$EC_{x_{mix}} = \left( \sum_{i=1}^n \frac{p_i}{EC_{x_i}} \right)^{-1} \quad (3)$$

where  $EC_{x_{mix}}$  is the total concentration of the mixture (in mg hesperetin equivalents/L) required to produce effect  $x$ ,  $n$  is the number of mixture components,  $p_i$  is the relative fraction of chemical  $i$  in the mixture, and  $EC_{x_i}$  is the concentration of  $i$  that produces effect  $x$  by itself. The  $p_i$  values of hesperetin, H-3'G, H-7G, hesperetin-3'-O-sulfate (H-3'S), and hesperetin-7-O-sulfate in total plasma concentrations of hesperetin (aglycone and metabolites) were predicted to be 0.01, 0.54, 0.32, 0.08, and 0.05 based on model stimulation (data not shown).

Before making the *in vitro* to *in vivo* translation, it is of importance to realise that hesperidin will bind to protein and lipid [48] and only the free fraction ( $f_u$ ) of the chemical will exert the effects, which implies a correction is required for differences between protein (predominantly albumin) and lipid (predominantly triglycerides, cholesterol, cholesterol ester, and phospholipid) binding in the *in vitro* bioassays and the *in vivo* situation. For the PKA inhibition activity that was performed using bioassay conditions without added protein and lipid, each nominal *in vitro* effect concentration ( $EC_{in\ vitro}$ ) was extrapolated to an *in vivo* effective concentration ( $EC_{in\ vivo}$ ) by dividing the  $EC_{in\ vitro}$  with the  $f_{u, in\ vivo}$  assuming 100% availability *in vitro*. The average  $f_{u, in\ vivo}$  of 0.27 for H-7G and H-3'G was used as approximately 70% of the total plasma hesperetin concentration (aglycone and metabolites) was predicted to be H-7G and H-3'G (Table 2 in the Supporting Information and Section 3.4). For *in vitro* activities that were obtained from *in vitro* bioassays performed in the presence of culture medium with added protein and lipid, each  $EC_{in\ vitro}$  was extrapolated to an  $EC_{in\ vivo}$  according to the extrapolation rule of G\u00fclden

**Table 1.** Kinetic constants for formation of hesperetin mono- and diconjugates obtained from in vitro incubations with relevant human tissue fractions

| Substrate                | Metabolites | Small intestine            |  |                                       |                  | Colon                      |  |                                       |                  | Liver                                     |  |                                       |                  |
|--------------------------|-------------|----------------------------|--|---------------------------------------|------------------|----------------------------|--|---------------------------------------|------------------|---|--|---------------------------------------|------------------|
|                          |             | $K_m$<br>( $\mu\text{M}$ ) | $V_{\text{max}}$ (nmol/min/<br>mg protein) | Scaled<br>$V_{\text{max}}^{\text{a}}$ | CE <sup>b)</sup> | $K_m$<br>( $\mu\text{M}$ ) | $V_{\text{max}}$ (nmol/min/<br>mg protein) | Scaled<br>$V_{\text{max}}^{\text{a}}$ | CE <sup>b)</sup> | $K_m$<br>( $\mu\text{M}$ )                | $V_{\text{max}}$ (nmol/min/<br>mg protein) | Scaled<br>$V_{\text{max}}^{\text{a}}$ | CE <sup>b)</sup> |
| Hesperetin <sup>d)</sup> | H-7G        | 8.3                        | 3.80                                       | 4.70                                  | 0.57             | 3.7                        | 1.55                                       | 0.22                                  | 0.06             | 20.1                                      | 8.00                                       | 19.20                                 | 0.96             |
|                          | H-3'G       | 6.4                        | 2.49                                       | 3.08                                  | 0.48             | 3.4                        | 0.99                                       | 0.14                                  | 0.04             | 10.6                                      | 6.96                                       | 16.70                                 | 1.58             |
|                          | H-7S        | 9.1                        | 0.14                                       | 0.15                                  | 0.02             | 8.6                        | 0.07                                       | 0.07                                  | 0.01             | 1.5                                       | 0.02                                       | 0.10                                  | 0.06             |
| H-7G <sup>e)</sup>       | H-3'S       | 0.6                        | 0.79                                       | 0.85                                  | 1.42             | 3.3                        | 0.2  | 0.20                                  | 0.06             | Strong substrate inhibition <sup>d)</sup> |  |                                       |                  |
|                          | H-73'diG    | 591                        | 0.47                                       | 0.58                                  | 0.001            | nd                         | nd   | –                                     | –                | 377                                       | 0.46                                       | 1.10                                  | 0.003            |
| H-3'G <sup>e)</sup>      | H-7G-3'S    | 49                         | 0.14                                       | 0.15                                  | 0.003            | nd                         | nd   | –                                     | –                | 25  | 0.07                                       | 0.34                                  | 0.01             |
|                          | H-3'7diG    | nd                         | nd   | –                                     | –                | nd                         | nd   | –                                     | –                | 270                                       | 0.03                                       | 0.07                                  | 0.0003           |
|                          | H-3'G-7S    | 45                         | 0.01                                       | 0.01                                  | 0.0002           | nd                         | nd   | –                                     | –                | nd  | nd   | –                                     | –                |

a)  $\mu\text{mol/h/g}$  tissue; calculated from  $V_{\text{max}}(\text{app})/(1000 \text{ nmol}/\mu\text{mol}) \times (60 \text{ min}) \times (\text{mg protein/g tissue})$ : small intestine protein content yield 20.6 mg/g tissue microsomes and 18 mg/g tissue cytosol [34], liver protein content yield 40 mg/g tissue microsomes and 80.7 mg/g tissue cytosol [35], and colonic protein content yield 2.4 mg/g tissue microsomes and 16.4 mg/g tissue cytosol (calculating based on the data report by Malfatti et al. [37] according to the method describe by van de Kerkhof et al. [36]).

b) In vivo catalytic efficiency (scaled  $V_{\text{max}}/K_m$ ) expressed as L/h/g tissue.

c) Kinetic constants for formation of hesperetin monoconjugates were obtained from Brand et al. [19].

d) Human liver cytosol showed strong H-3'S substrate inhibition at concentration  $>0.1 \mu\text{M}$ , hampering determination of kinetic constants for this reaction [19].

e) Kinetic constants for formation of hesperetin diconjugates were obtained in the present study. For full concentration-dependent activity curves from which these kinetic constants are derived, see Fig. 1 in the Supporting Information.

nd, not detected.

and Seibert as follows [49]:

$$EC_{in\ vivo} = EC_{in\ vitro} \times \left[ (1 - fb_{in\ vitro}) \times \frac{1 + K_{OW} \times V'_{L,serum}}{1 + K_{OW} \times V'_{L,in\ vitro}} + fb_{in\ vitro} \times \frac{P_{serum}}{P_{in\ vitro}} \right] \quad (4)$$

where  $fb_{in\ vitro}$  is the fraction of chemical bound to protein and lipid in culture medium, which is calculated from  $1 - fu_{in\ vitro}$ .  $V'_L$  is the lipid fraction in serum and in vitro.  $P$  is the protein content in serum and culture medium.

For the extrapolation, in vivo albumin and lipid concentrations of 600  $\mu\text{M}$  and 6 g/L were used [49]. The albumin and lipid concentrations in culture medium of the reported in vitro bioassays were estimated from the reported data by Glden et al. [50] indicating that 5% foetal bovine serum contains 18  $\mu\text{M}$  bovine serum albumin and 0.1 g/L lipid. The  $fu_{in\ vitro}$  values of hesperetin and its metabolites in in vitro medium were estimated using the reported binding constant of hesperetin, H-7G, and H-3'G to human serum albumin of 8, 4, and  $6 \times 10^4 \text{ M}^{-1}$  [48] and a binding site number of 1.05 [51], assuming a similar binding constant for human and bovine serum albumin. This assumption is based on the fact that genistein has been reported to have a similar binding constant for bovine and human serum albumin [52]. The in vivo effect concentration of the mixtures obtained after correction for difference in protein and lipid between the in vitro and in vivo situation was set equal to plasma  $C_{max}$  of the mixtures in the PBK model to predict the corresponding oral dose level in humans. The 95% lower and upper confidence limit of the in vivo dose–response curves were estimated from the derived in vivo dose–response curve using GraphPad Prism version 5.04 (GraphPad Software). The data points of the derived 95% lower and upper confidence limit in vivo dose–response curves were digitized using Plot Digitizer version 2.5.1 (Joseph A. Huwaldt, Sourceforge.net). Subsequently, the digitized data thus obtained were used to estimate the benchmark dose for 5% response ( $BMD_{05}$ ) based on the default benchmark response for continuous data [53]. The  $BMD_{05}$  values were estimated by fitting to the Hill model using Benchmark Dose Software version 2.6 (The Environment Protection Agency's, USA). The  $BMD_{05}$  values obtained were evaluated against reported active human data on antiatherogenic and anti-inflammatory activity upon oral intake of hesperidin [54–56].

### 3 Results

#### 3.1 Enzymatic conjugation of H-7G and H-3'G in incubations with human tissue fractions

Analysis of glucuronidation incubations of H-7G and H-3'G containing pooled human tissue fractions revealed that

H-7G was further glucuronidated by human small intestine and liver microsomes, revealing one metabolite that is formed, whereas H-3'G was only further glucuronidated by human liver microsomes, resulting in the same metabolite as observed from the incubations with H-7G. This metabolite coeluted with and showed similar spectral characteristics as commercially available H-3'7diG and could thus be identified as H-3'7diG. Under the conditions of the present study, no glucuronidated metabolites of H-7G or H-3'G were formed in incubations containing human colon S9.

Analysis of sulfation incubations of H-7G and H-3'G containing pooled human tissue fractions revealed that H-7G was further sulfated by human small intestine and liver cytosol, while H-3'G was only further sulfated by human small intestine cytosol. The metabolites formed in the sulfation incubations with H-7G and H-3'G with a retention time of 1.3 and 1.4 min were identified by treating the un-terminated samples with  $\beta$ -glucuronidase/sulfatase resulting in a disappearance of the respect peak and a concomitant equivalent increase in the peak area of hesperetin aglycone (data not shown). These results confirm that the metabolites were most likely hesperetin-7-O-glucuronide-3'-O-sulfate (H-7G-3'S) and hesperetin-3'-O-glucuronide-7-O-sulfate because conjugation of the flavonoid likely occurs at available free OH moieties [57] and the five position is not available for conjugation due to intramolecular hydrogen bonding with the carbonyl group at the C-4 position [58]. Under the conditions of the present study, no sulfated metabolites of H-7G and H-3'G formed in incubations with human colon S9 were detected.

#### 3.2 Kinetic constants for formation of mono- and diconjugates of hesperetin

The concentration-dependent rates of glucuronidation and sulfation of H-7G and H-3'G by human tissue fractions are shown in Fig. 1 in the Supporting Information. The kinetic constants derived from these results and the kinetic constants for formation of different hesperetin monoconjugates obtained from Brand et al. [19] are summarized in Table 1. The results indicate that small intestine and liver had similar catalytic efficiency for metabolism of hesperetin with the total catalytic efficiency amounting to approximately 2.5 L/h/g tissue for both tissues, followed by colon with a total catalytic efficiency of 0.17 L/h/g tissue. Small intestine and liver tissues showed a difference in the type of conjugation of hesperetin as small intestine appeared to be especially effective in formation of H-3'S, whereas liver was more effective in converting hesperetin into H-3'G. The formation of diconjugates was more than 100-fold less efficient than the formation of the respective monoconjugates due to a decrease in  $V_{max}$  and an increase in  $K_m$  values. Colon could only covert hesperetin to monoconjugates as there was no formation of diconjugates detected in incubations with this tissue fraction.

### 3.3 PBK model development and evaluation

The PBK model for hesperidin consisted of separate compartments for GI tract lumen, small intestine, colon, liver, kidney, and blood, which are the major organs involved in ADME of hesperidin and its metabolites (Fig. 2A and B). The remaining organs are lumped to either rapidly perfused tissues (e.g. heart, lung, brain) or slowly perfused tissues (e.g. skin, muscle, bone). To define the PBK model, kinetic parameters for formation of different hesperetin mono- and diconjugates were obtained from *in vitro* incubations. While the hydrolytic clearance of hesperidin by gut microbiota and the kinetic parameters for excretion via urine, bile, and intestinal efflux back to intestinal lumen were obtained by fitting the predicted dose-dependent plasma concentrations of total hesperetin concentrations with available experimental human data in plasma [13, 15, 16, 28–30], resulting in values of 0.1 L/h, 30 h<sup>-1</sup>, 30 h<sup>-1</sup>, and 0.2 L/h, respectively. Subsequently, the model thus defined was used to predict the total hesperetin plasma kinetics as shown in Fig. 3. Twenty-four out of 30 predictions on plasma C<sub>max</sub>, area under the time–response curve, and T<sub>max</sub> of total hesperetin were within twofold deviation from the reported human data [13, 15, 16, 28–30], whereas the rest of the predictions were within three- to sixfold deviation. The reason for this discrepancy might be due to interindividual human variation in metabolism of hesperetin, especially for the parameters of influence that were defined by the sensitivity analysis.

The performance of the defined PBK model was evaluated to a further extent by comparing the predicted concentrations of hesperetin metabolites excreted in urine to the reported literature data for hesperetin metabolites in human urine [1, 13, 42]. Figure 4 shows the results of this comparison revealing that the model adequately predicted the urinary profiles of different mono- and diconjugates of hesperetin as 20 of 27 of the predicted values for excretion of hesperetin metabolites were within twofold deviation from the reported urinary profiles of hesperetin metabolites in humans [1, 13, 42], whereas the others were within four- to sevenfold deviation. The reason for this discrepancy might be due to interindividual human variation in metabolism of hesperetin, especially for the parameters of influence that were defined by the sensitivity analysis.

To further evaluate the performance of the defined model, a sensitivity analysis was performed to assess key parameters that influence the predicted plasma C<sub>max</sub> of hesperetin aglycone and its metabolites at an oral dose of 2.8 and 29 mg/kg bw hesperidin representing the lowest and the highest hesperidin intake originating from the Western diet and from food supplements, respectively [17, 18]. Only parameters that had a normalized SC higher than 0.1 (in absolute value) are shown in Fig. 2 in the Supporting Information. The results reveal that the normalized SCs of most of the PBK model parameters were not dose dependent. The predicted plasma C<sub>max</sub> of hesperetin aglycone and its metabolites are mainly influenced by the body weight, the volume of the GI tract

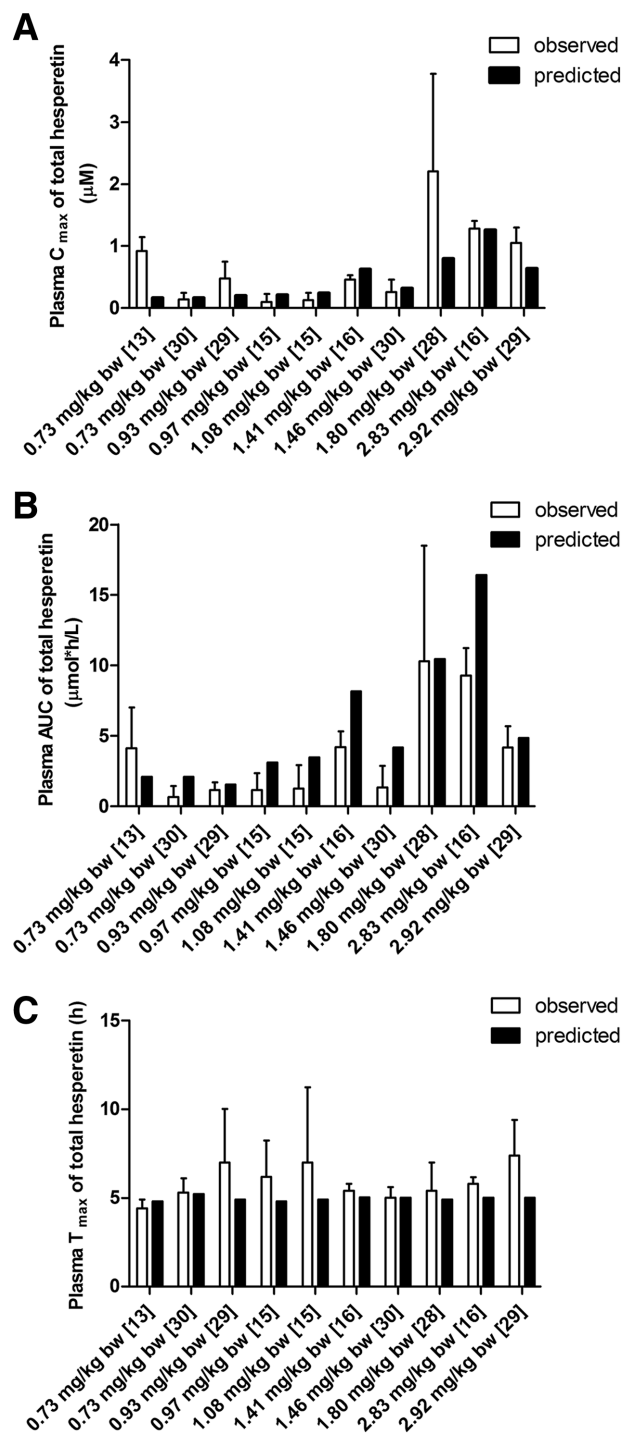


**Figure 3.** Observed and PBK model-predicted (A) plasma C<sub>max</sub>, (B) plasma area under the time–response curve (AUC), and (C) plasma T<sub>max</sub> of total hesperetin (aglycone and metabolites) in humans at different dose levels as indicated by the x-axis labels [13, 15, 16, 28–30]. Data sets presented represent dose regimens for which observed values were reported in the literature.

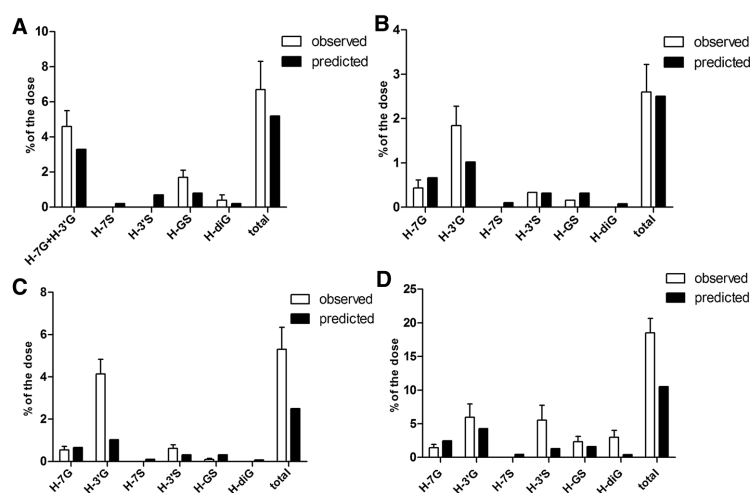


**Figure 4.** Model evaluation by comparing the PBK model-predicted urinary profiles with those reported by (A) Mullen et al. at 0.73 mg/kg bw hesperidin [13], (B) Bredsdorff et al. at 0.93 mg/kg bw hesperidin [42], (C) Bredsdorff et al. at 2.92 mg/kg bw hesperidin [42], and (D) Pereira-Caro et al. at 2.87 mg/kg bw hesperidin [1]. Data sets presented represent dose regimens for which observed values were reported in the literature. Since the literature study reporting observed levels for H-GS did not discriminate between hesperetin-3'-O-glucuronide-7-O-sulfate (H-3'G-7S) and H-7G-3'S, H-GS represents both conjugates.

lumen and liver, the regional blood flow through the small intestine and colon, the blood to plasma ratio, and the biliary excretion (expressing normalized SCs between 0.5 and 2.6 in absolute value). The parameters that influenced the formation of hesperetin monoconjugates in the colon and liver, including the microsomal and cytosol protein contents in the colon and liver and the kinetic constants for formation of monoconjugates, are also influential parameters for the predicted plasma  $C_{max}$  of hesperetin aglycone and its metabolites (expressing normalized SCs between 0.2 and 0.9 in absolute value). In addition, the kinetic constants for formation of H-3'7diG and H-7G-3'S in the liver and the kinetic constants for formation of hesperetin-3'-O-glucuronide-7-O-sulfate and the cytosol protein content in the small intestine are also influential parameters for the predicted plasma  $C_{max}$  of its respective diconjugates (expressing normalized SCs between 0.3 and 2.0 in absolute value).

### 3.4 PBK model predictions of metabolic plasma profiles of hesperidin

The PBK model was used to predict metabolic plasma profiles of hesperidin at different dose levels. Figure 5 shows the predicted dose-dependent plasma concentrations of hesperetin aglycone and its metabolites (expressed in mg hesperetin equivalents/L) at oral doses ranging from 0.01 to 50 mg/kg bw hesperidin, revealing that the conjugation pattern of the circulating metabolites does not change with the dose. At all oral doses, H-3'G and H-7G were predicted to be the major circulating metabolites together accounting for approximately 70% of the total plasma hesperetin concentration (aglycone and metabolites), followed by H-7G-3'S, H-3'S, and H-3'7diG accounting for approximately 15, 6, and 4% of the total plasma hesperetin concentration, respectively. Hesperetin aglycone was present at a low concentration below 0.02 mg/L at a dose of 50 mg/kg bw and accounted for approximately 0.5% of the total plasma hesperetin concentration at all oral doses.

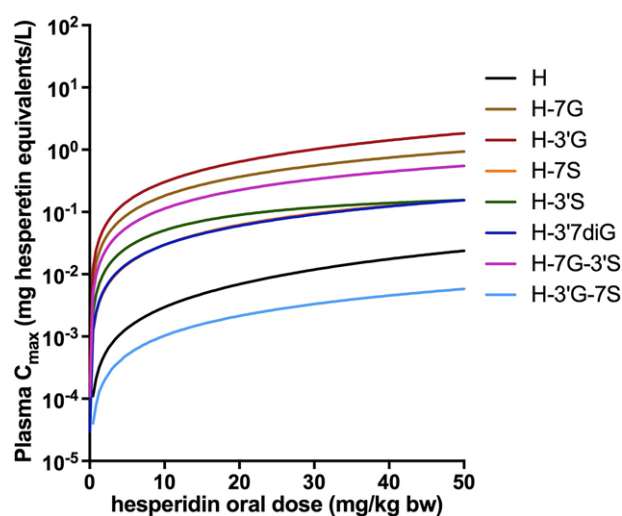


**Figure 5.** PBK model based prediction of the dose-dependent plasma  $C_{max}$  of hesperetin aglycone and its metabolites at oral doses ranging from 0.01 to 50 mg/kg bw hesperidin: hesperetin (H), glucuronide (G), and sulfate (S).

### 3.5 Translation of in vitro effect concentrations to in vivo effective dose levels in human

In the next step, the PBK model was used for reverse dosimetry converting in vitro effective concentrations to in vivo effective dose levels of hesperidin for selected endpoints. To this end, in vitro concentration–response curves were defined in first instance for PKA inhibition by hesperetin, H-3'G, and H-7G in the present study. The results obtained reveal that hesperetin and also its major circulating metabolites, H-3'G, and H-7G, all inhibit PKA activity in vitro in a concentration-dependent manner as shown in the left panel of Fig. 6A. This figure, reflecting the in vitro concentration–response curves for PKA inhibition by hesperetin, H-3'G, and H-7G (left panel of Fig. 6A), also depicts as a first approximation

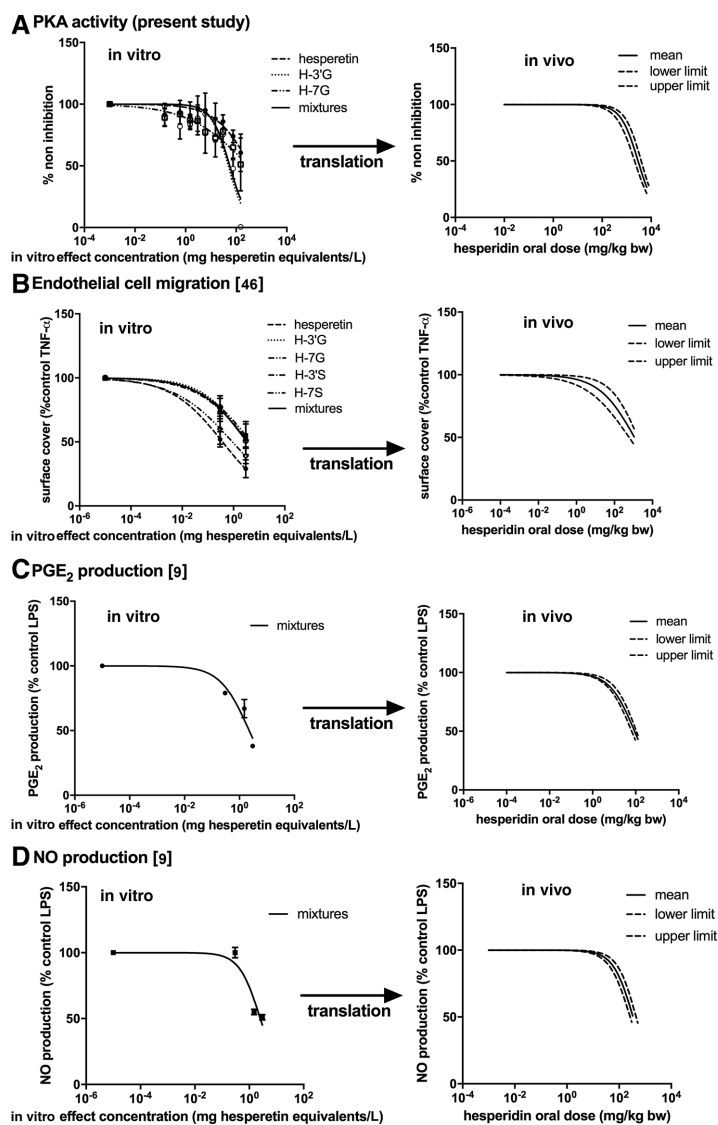


**Figure 6.** Translation of *in vitro* concentration–response curves for (A) inhibition of PKA activity (present study), (B) inhibition of endothelial cell migration [46], (C) inhibition of LPS-induced prostaglandin E<sub>2</sub> (PGE<sub>2</sub>) production [9], and (D) inhibition of LPS-induced nitric oxide (NO) production [9] to human hesperidin dose–response curves using PBK model based reverse dosimetry based on plasma C<sub>max</sub> of total hesperetin (aglycone and metabolites). For inhibition of LPS-induced PGE<sub>2</sub> and NO production, *in vitro* studies for these endpoints were carried out with mixtures of hesperetin metabolites, not individual metabolites, and thus only the mixtures concentration–response curves are presented (C and D left panel) [9].

the concentration–response curves for PKA inhibition by combined exposure to the mixtures of hesperetin, H-3'G, and H-7'G, assuming the three compounds to be present at the ratios predicted to be present in plasma, and using the concentration–response curves for the individual compounds, expressing the concentration of the mixture in mg hesperetin equivalents/L. Figure 6B–D (left panels) presents similar *in vitro* data for the effect of hesperetin and its conjugates on other endpoints including effects on inhibition of cell migration induced by TNF- $\alpha$  (Fig. 6B left panel), inhibition of PGE<sub>2</sub> production induced by LPS (Fig. 6C left panel), and inhibition of NO production induced by LPS (Fig. 6D left panel). The latter two Figs 6(C and D left panel) only present the *in vitro* concentration–response curves for the mixtures (mainly monoconjugates) as *in vitro* studies for these endpoints were carried out with mixtures of hesperetin metabolites obtained from rat plasma exposed to 50 mg/kg bw

hesperetin [9]. The major circulating metabolites of hesperetin in rat exposed to 50 mg/kg bw hesperidin were reported to be monoglucuronides followed by mixed conjugates containing glucuronic acid and sulfate moieties [59], which is comparable to the predicted metabolic plasma profiles in humans (Section 3.4). In a subsequent step, these *in vitro* concentration–response curves were translated into *in vivo* dose–response curves using a PBK model based reverse dosimetry. To this end, each *in vitro* mixture concentration was extrapolated to an *in vivo* mixtures concentration in plasma by taking into account the differences in protein and lipid concentration between the *in vitro* bioassays and the *in vivo* situations (see Section 2.6). The plasma *in vivo* concentrations of the mixtures of hesperetin and its metabolites thus obtained were used as input in the PBK model to predict the *in vivo* dose levels of hesperidin required to achieve these plasma concentrations,

deriving the in vivo dose–response curve. Figure 6 (right panels) depicts the in vivo dose–response curves obtained. The figures also present the 95% lower and upper confidence limits of the predicted in vivo dose–response curves. Subsequently, the obtained in vivo dose–response curves were used to estimate the BMD<sub>05</sub> values for the respective biological effect of hesperidin in humans. In this way, the BMD<sub>05</sub> values for several biological effects including inhibition of PKA, inhibition of cell migration induced by TNF- $\alpha$ , inhibition of PGE<sub>2</sub> production induced by LPS, and inhibition of NO production induced by LPS were predicted using a PBK model based reverse dosimetry.

Figure 7 shows the predicted in vivo BMD<sub>05</sub> values based on in vitro data for the inhibition of PKA activity by hesperetin and its metabolites, endothelial cell migration, and induction of PGE<sub>2</sub> and NO. The in vivo BMD<sub>05</sub> values for PKA inhibition were predicted to occur at oral doses ranging from 135 to 539 mg/kg bw hesperidin. The in vivo BMD<sub>05</sub> values for inhibition of endothelial cell migration were predicted to occur at oral doses ranging from 4.54 to 24 mg/kg bw hesperidin. The in vivo BMD<sub>05</sub> values for inhibition of PGE<sub>2</sub> production were predicted to occur at oral doses ranging from 2.19 to 4.10 mg/kg bw hesperidin. And the in vivo BMD<sub>05</sub> values for inhibition of NO production were predicted to occur at oral doses ranging from 17 to 44 mg/kg bw hesperidin.

The predicted in vivo BMD<sub>05</sub> values for effects of hesperetin and its metabolites on PKA activity, endothelial cell migration, PGE<sub>2</sub> production, and NO production based on the in vitro PBK approach were evaluated by comparing the predicted in vivo BMD<sub>05</sub> values with the reported active dose levels of hesperidin on anti-atherogenic and anti-inflammatory effects in healthy humans [54–56] as PKA regulates several cellular functions [23], endothelial cell migration is an initiated bioprocess for atherosclerosis [46], and PGE<sub>2</sub> and NO are inflammatory biomarkers [9]. The results as shown in Fig. 7 reveal that the predicted in vivo BMD<sub>05</sub> values for inhibition of endothelial cell migration and PGE<sub>2</sub> production are in line with the active dose levels of hesperidin (4.2 mg/kg bw) in human intervention studies reported to result in improved endothelial function and decreased levels of inflammatory biomarkers (i.e. PGE<sub>2</sub> and C-reactive protein) [54–56]. The predicted in vivo BMD<sub>05</sub> values for inhibition of NO production are four to tenfold higher than the reported active dose levels of hesperidin in humans [54–56]. In the case of PKA activity, the predicted in vivo BMD<sub>05</sub> values are more than 32-fold higher than the reported active dose levels of hesperidin on anti-atherogenic and anti-inflammatory effects of hesperidin in humans [54–56].

The PBK model based predicted dose–response curves and in vivo BMD<sub>05</sub> values derived from them also indicate that at a Western dietary and a supplementary intake of hesperidin amounting to 2.8–8 and 7–29 mg/kg bw, respectively [17, 18], the plasma C<sub>max</sub> of total hesperetin would be high enough to inhibit endothelial cell migration, PGE<sub>2</sub> production, and NO production (Fig. 7).

## 4 Discussion

The aim of the present study was to develop a PBK model describing the ADME of hesperidin in humans to obtain insight in dose-dependent plasma concentrations of hesperetin aglycone and its circulating metabolites and to subsequently combine the developed PBK model with in vitro effect concentrations to determine whether and if so at what oral dose levels the in vitro effects of hesperetin and its metabolites may actually occur in vivo. Evaluation of the PBK model developed against literature reported data on plasma kinetics and urinary profiles of hesperidin reveals that the model adequately predicted plasma kinetics of total hesperetin and urinary profiles of hesperidin within one- to sevenfold deviation. The model developed was used to predict the dose-dependent plasma concentrations of hesperetin aglycone as well as the type of circulating metabolites. The results revealed that the metabolic plasma profiles of hesperidin appear independent of the dose because similar circulating metabolite patterns of hesperetin were predicted at all dose levels from 0.01 to 50 mg/kg bw hesperidin. The model predicted that H-3'G and H-7G were the major circulating metabolites of hesperidin and that the plasma concentrations of hesperetin aglycone were limited and predicted to be lower than 0.02 mg/L even at an oral dose of 50 mg/kg bw hesperidin. This implies that in vivo effects of hesperidin would probably have to be at least in part ascribed to hesperetin metabolites including H-3'G and H-7G.

Given that hesperidin was predicted to be present in the systemic circulation mainly in the form of conjugated metabolites, it is crucial to understand the biological activity of these conjugates in order to gain more insight in possible in vivo effects of hesperidin. The in vitro data on PKA inhibition of hesperetin and its major circulating metabolites H-3'G and H-7G showed that the two metabolites were at least equally active in inhibition of PKA as hesperetin aglycone. Yang *et al.* reported that at the same concentration mixtures of hesperetin metabolites (mainly monoconjugates) exhibited approximately twofold higher inhibition of PGE<sub>2</sub> and NO production as compared with hesperetin aglycone in LPS-stimulated RAW 264.7 [9]. Hesperetin monoconjugates were also reported to exert inhibition activity on cell migration in TNF- $\alpha$  treated human aortic endothelial cell with approximately 1.5-fold lower potency than hesperetin aglycone at the same concentration [46]. Overall, this points out that conjugation does not necessarily result in loss or reduction of the biological activity and in vivo effects of hesperidin are at least in part due to its metabolites. Based on these results it was decided that in a first approximation the concentrations of hesperetin and its metabolites could be added up for evaluation of how the in vitro effect concentrations translate into the in vivo hesperidin dose level.

The PBK model developed provided a unique tool to gain more insight in how the in vitro concentrations translate into in vivo dose levels of hesperidin by applying PBK model based

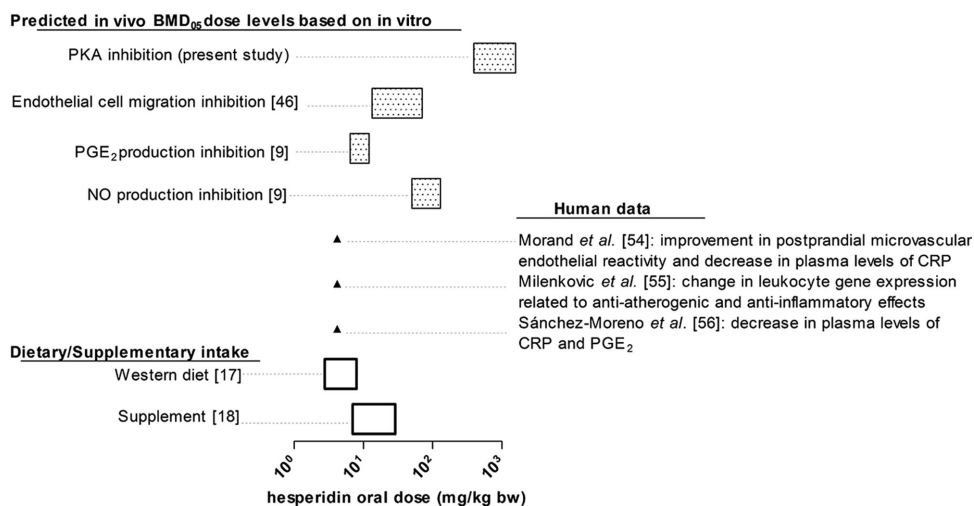


**Figure 7.** Comparison of the predicted in vivo BMD<sub>05</sub> values of hesperidin derived from in vitro effects of the mixtures of hesperetin and its metabolites on inhibition of PKA activity (present study), endothelial cell migration [46], prostaglandin E<sub>2</sub> (PGE<sub>2</sub>) production [9], and nitric oxide (NO) production [9] with the reported active dose levels on anti-atherogenic and anti-inflammatory effects of hesperidin in humans [54–56] and with a Western dietary [17] and a supplementary [18] intake of hesperidin.

reverse dosimetry. The in vivo dose–response curves obtained were used to derive the BMD<sub>05</sub> values at which plasma concentrations of hesperetin together with its metabolites would be high enough to exert 5% response for inhibition of PKA activity, inhibition of TNF- $\alpha$  induced endothelial cell migration, inhibition of LPS induced PGE<sub>2</sub> production, and inhibition of LPS-induced NO production. The predicted in vivo BMD<sub>05</sub> values for PKA inhibition ranged from 135 to 539 mg/kg bw hesperidin. The predicted in vivo BMD<sub>05</sub> values for inhibition of TNF- $\alpha$ -induced endothelial cell migration ranged from 4.54 to 24 mg/kg bw hesperidin. The predicted in vivo BMD<sub>05</sub> values for inhibition of LPS-induced PGE<sub>2</sub> production ranged from 2.19 to 4.10 mg/kg bw hesperidin. And in the case of LPS-induced NO production, the in vivo BMD<sub>05</sub> values for inhibition ranged from 17 to 44 mg/kg bw hesperidin. These predictions were evaluated against the reported active dose levels of hesperidin for anti-atherogenic and anti-inflammatory effect as reported in humans [54–56]. The predicted in vivo BMD<sub>05</sub> values for inhibition of endothelial cell migration and PGE<sub>2</sub> production are in line with the reported active dose levels of hesperidin in humans for improving endothelial function and decreasing levels of inflammatory biomarkers (i.e. PGE<sub>2</sub> and C-reactive protein) [54–56]. The predicted in vivo BMD<sub>05</sub> values for inhibition of NO production are four- to tenfold higher than the reported active dose levels of hesperidin in humans [54–56]. The predicted in vivo BMD<sub>05</sub> values for PKA inhibition are more than 32-fold higher than the reported active dose levels for anti-atherogenic and anti-inflammatory effects of hesperidin in humans [54–56]. This might imply that inhibition of PKA activity (a regulator of several cellular functions [23]) is not a major mechanism for anti-atherogenic and anti-inflammatory action of hesperidin in vivo.

Based on the predicted in vivo BMD<sub>05</sub> values for hesperidin derived from in vitro concentration–response curves for hesperidin-mediated inhibition of PKA activity, TNF- $\alpha$  induced endothelial cell migration, and LPS-induced production of PGE<sub>2</sub> and NO, it can also be concluded that the plasma

C<sub>max</sub> of total hesperetin (aglycone and metabolites) at a Western dietary and a supplementary intake amounting to 2.8–8 [17] and 7–29 [18] mg/kg bw hesperidin would be high enough to induce these effects on endothelial cell migration and pro-inflammatory molecules *in vivo*. For the inhibition of PKA activity, the plasma C<sub>max</sub> of total hesperetin upon these dietary or supplementary intakes would generally not be high enough to induce a similar effect on PKA activity in vivo.

Overall, the PBK model developed in the present study adequately predicted ADME of hesperidin in humans. The model obtained was also shown to be of use to translate in vitro results on the biological effects of hesperetin aglycone and its metabolites to the human in vivo situation and evaluate the possible occurrence of in vivo effects without the need for human intervention studies.

R.B. and A.S. performed experiments. R.B. analyzed data. R.B., A.P., and I.R. wrote and edited the manuscript. All authors read and approved the final manuscript.

This research was financially supported by the Ministry of Science and Technology of Thailand through a Royal Thai Government Scholarship awarded to Rungnapa Boonpawa for conducting her PhD in The Netherlands.

The authors have declared no conflict of interest.

## 5 References

- [1] Pereira-Caro, G., Borges, G., van der Hooft, J., Clifford, M. N. et al., Orange juice (poly)phenols are highly bioavailable in humans. *Am. J. Clin. Nutr.* 2014, 100, 1378–1384.
- [2] Tomás-Barberán, F. A., Clifford, M. N., Flavanones, chalcones and dihydrochalcones—nature, occurrence and dietary burden. *J. Sci. Food Agric.* 2000, 80, 1073–1080.
- [3] Roohbakhsh, A., Parhiz, H., Soltani, F., Rezaee, R. et al., Molecular mechanisms behind the biological effects of hesperidin and hesperetin for the prevention of cancer and cardiovascular diseases. *Life Sci.* 2015, 124, 64–74.

- [4] Chiba, H., Kim, H., Matsumoto, A., Akiyama, S. et al., Hesperidin prevents androgen deficiency-induced bone loss in male mice. *Phytother. Res.* 2014, *28*, 289–295.
- [5] Kawser Hossain, M., Abdal Dayem, A., Han, J., Yin, Y. et al., Molecular mechanisms of the anti-obesity and anti-diabetic properties of flavonoids. *Int. J. Mol. Sci.* 2016, *17*, 569.
- [6] Smina, T. P., Mohan, A., Ayyappa, K. A., Sethuraman, S. et al., Hesperetin exerts apoptotic effect on A431 skin carcinoma cells by regulating mitogen activated protein kinases and cyclins. *Cell Mol. Biol.* 2015, *61*, 92–99.
- [7] Choi, E. J., Hesperetin induced G1-phase cell cycle arrest in human breast cancer MCF-7 cells: involvement of CDK4 and p21. *Nutr. Cancer* 2007, *59*, 115–119.
- [8] Palit, S., Kar, S., Sharma, G., Das, P. K., Hesperetin induces apoptosis in breast carcinoma by triggering accumulation of ROS and activation of ASK1/JNK pathway. *J. Cell Physiol.* 2015, *230*, 1729–1739.
- [9] Yang, H.-L., Chen, S.-C., Senthil Kumar, K. J., Yu, K.-N. et al., Antioxidant and anti-inflammatory potential of hesperetin metabolites obtained from hesperetin-administered rat serum: an ex vivo approach. *J. Agric. Food Chem.* 2012, *60*, 522–532.
- [10] Chanet, A., Milenkovic, D., Claude, S., Maier, J. A. M. et al., Flavanone metabolites decrease monocyte adhesion to TNF- $\alpha$ -activated endothelial cells by modulating expression of atherosclerosis-related genes. *Br. J. Nutr.* 2013, *110*, 587–598.
- [11] Kim, G. D., Hesperetin inhibits vascular formation by suppressing of the PI3K/AKT, ERK, and p38 MAPK signaling pathways. *Prev. Nutr. Food Sci.* 2014, *19*, 299–306.
- [12] Trzeciakiewicz, A., Habauzit, V., Mercier, S., Barron, D. et al., Molecular mechanism of hesperetin-7-O-glucuronide, the main circulating metabolite of hesperidin, involved in osteoblast differentiation. *J. Agric. Food Chem.* 2009, *58*, 668–675.
- [13] Mullen, W., Archeveque, M.-A., Edwards, C. A., Matsumoto, H. et al., Bioavailability and metabolism of orange juice flavanones in humans: impact of a full-fat yogurt. *J. Agric. Food Chem.* 2008, *56*, 11157–11164.
- [14] Takumi, H., Nakamura, H., Simizu, T., Harada, R. et al., Bioavailability of orally administered water-dispersible hesperetin and its effect on peripheral vasodilatation in human subjects: implication of endothelial functions of plasma conjugated metabolites. *Food Funct.* 2012, *3*, 389–398.
- [15] Brett, G. M., Hollands, W., Needs, P. W., Teucher, B. et al., Absorption, metabolism and excretion of flavanones from single portions of orange fruit and juice and effects of anthropometric variables and contraceptive pill use on flavanone excretion. *Br. J. Nutr.* 2009, *101*, 664–675.
- [16] Manach, C., Morand, C., Gil-Izquierdo, A., Bouteloup-Demange, C. et al., Bioavailability in humans of the flavanones hesperidin and narirutin after the ingestion of two doses of orange juice. *Eur. J. Clin. Nutr.* 2003, *57*, 235–242.
- [17] Koch, W., Kukuła-Koch, W., Marzec, Z., Marć, D., Application of TLC method with video scanning in estimation of daily dietary intake of specific flavonoids-preliminary studies. *Acta Pol. Pharm.* 2013, *70*, 611–620.
- [18] Hendler, S. S., Rorvik, D. M., *PDR for Nutritional Supplements*, 2nd ed, Thomson Reuters, New Jersey 2008.
- [19] Brand, W., Boersma, M. G., Bik, H., Hoek-van den Hil, E. F. et al., Phase II metabolism of hesperetin by individual UDP-glucuronosyltransferases and sulfotransferases and rat and human tissue samples. *Drug. Metab. Dispos.* 2010, *38*, 617–625.
- [20] Perche, O., Vergnaud-Gauduchon, J., Morand, C., Dubray, C. et al., Orange juice and its major polyphenol hesperidin consumption do not induce immunomodulation in healthy well-nourished humans. *Clin. Nutr.* 2013, *33*, 130–135.
- [21] Oleson, L., Court, M. H., Effect of the  $\beta$ -glucuronidase inhibitor saccharolactone on glucuronidation by human tissue microsomes and recombinant UDP-glucuronosyltransferases (UGTs). *J. Pharm. Pharmacol.* 2008, *60*, 1175–1182.
- [22] Wright, B., Watson, K. A., McGuffin, L. J., Lovegrove, J. A. et al., GRID and docking analyses reveal a molecular basis for flavonoid inhibition of Src family kinase activity. *J. Nutr. Biochem.* 2015, *26*, 1156–1165.
- [23] Howe, A. K., Regulation of actin-based cell migration by cAMP/PKA. *Biochim. Biophys. Acta* 2004, *1692*, 159–174.
- [24] Chen, N., Yang, H., Niu, J., Liu, S., Determination of kinetic parameters and structure-activity relationships of ginsenosides as inhibitors of cyclin-dependent kinase 5/p25 using ultra-pressure liquid chromatography with triple quadrupole tandem mass spectrometry. *Rapid. Commun. Mass. Spectrom.* 2013, *27*, 985–992.
- [25] Meggio, F., Deana, A. D., Ruzzene, M., Brunati, A. M. et al., Different susceptibility of protein kinases to staurosporine inhibition. *Eur. J. Biochem.* 1995, *234*, 317–322.
- [26] Boonpawa, R., Spengelink, A., Rietjens, I. M. C. M., Punt, A., A physiologically based kinetic (PBK) model describing plasma concentrations of quercetin and its metabolites in rats. *Biochem. Pharmacol.* 2014, *89*, 287–299.
- [27] Boonpawa, R., Moradi, N., Spengelink, A., Rietjens, I. M. C. M. et al., Use of physiologically based kinetic (PBK) modeling to study interindividual human variation and species differences in plasma concentrations of quercetin and its metabolites. *Biochem. Pharmacol.* 2015, *98*, 690–702.
- [28] Erlund, I., Meririnne, E., Alfthan, G., Aro, A., Plasma kinetics and urinary excretion of the flavanones naringenin and hesperetin in humans after ingestion of orange juice and grapefruit juice. *J. Nutr.* 2001, *131*, 235–241.
- [29] Nielsen, I. L. F., Chee, W. S. S., Poulsen, L., Offord-Cavin, E. et al., Bioavailability is improved by enzymatic modification of the citrus flavonoid hesperidin in humans: a randomized, double-blind, crossover trial. *J. Nutr.* 2006, *136*, 404–408.
- [30] Gardana, C., Guarnieri, S., Riso, P., Simonetti, P. et al., Flavanone plasma pharmacokinetics from blood orange juice in human subjects. *Br. J. Nutr.* 2007, *98*, 165–172.
- [31] Silberberg, M., Morand, C., Mathevon, T., Besson, C. et al., The bioavailability of polyphenols is highly governed by the capacity of the intestine and of the liver to secrete conjugated metabolites. *Eur. J. Nutr.* 2006, *45*, 88–96.
- [32] Steensma, A., Noteborn, H. P. J. M., Kuiper, H. A., Comparison of Caco-2, IEC-18 and HCEC cell lines as a model for

- intestinal absorption of genistein, daidzein and their glycosides. *Environ. Toxicol. Pharmacol.* 2004, *16*, 131–139.
- [33] Kimura, T., Higaki, K., Gastrointestinal transit and drug absorption. *Biol. Pharm. Bull.* 2002, *25*, 149–164.
- [34] Cubitt, H., Houston, J. B., Galetin, A., Relative importance of intestinal and hepatic glucuronidation—impact on the prediction of drug clearance. *Pharm. Res.* 2009, *26*, 1073–1083.
- [35] Cubitt, H. E., Houston, J. B., Galetin, A., Prediction of human drug clearance by multiple metabolic pathways: integration of hepatic and intestinal microsomal and cytosolic data. *Drug. Metab. Dispos.* 2011, *39*, 864–873.
- [36] van de Kerkhof, E. G., de Graaf, I. A. M., Groothuis, G. M. M., *In vitro* methods to study intestinal drug metabolism. *Curr. Drug Metab.* 2007, *8*, 658–675.
- [37] Malfatti, M. A., Connors, M. S., Mauthe, R. J., Felton, J. S., The capability of rat colon tissue slices to metabolize the cooked-food carcinogen 2-amino-1-methyl-6-phenylimidazo[4,5-b]pyridine. *Cancer Res.* 1996, *56*, 2550–2555.
- [38] Brown, R. P., Delp, M. D., Lindstedt, S. L., Rhomberg, L. R. et al., Physiological parameter values for physiologically based pharmacokinetic models. *Toxicol. Ind. Health* 1997, *13*, 407–484.
- [39] DeJongh, J., Verhaar, H. J. M., Hermens, J. L. M., A quantitative property-property relationship (QPPR) approach to estimate *in vitro* tissue-blood partition coefficients of organic chemicals in rats and humans. *Arch. Toxicol.* 1997, *72*, 17–25.
- [40] Simcyp. Simcyp prediction tools—fu. [Online]. 2014. Available from: <https://members.simcyp.com/account/tools/fu/>.
- [41] Simcyp. Simcyp prediction tools—blood to plasma partition ratio (B/P). [Online]. 2014. Available from: <https://members.simcyp.com/account/tools/BP/>.
- [42] Bredsdorff, L., Nielsen, I. L. F., Rasmussen, S. E., Cornett, C. et al., Absorption, conjugation and excretion of the flavanones, naringenin and hesperetin from  $\alpha$ -rhamnosidase-treated orange juice in human subjects. *Br. J. Nutr.* 2010, *103*, 1602–1609.
- [43] Evans, M. V., Andersen, M. E., Sensitivity analysis of a physiological model for 2,3,7,8-Tetrachlorodibenzo-p-dioxin (TCDD): assessing the impact of specific model parameters on sequestration in liver and fat in the rat. *Toxicol. Sci.* 2000, *54*, 71–80.
- [44] Louisse, J., Bosgra, S., Blaauboer, B., Rietjens, I. C. M. et al., Prediction of *in vivo* developmental toxicity of all-trans-retinoic acid based on *in vitro* toxicity data and *in silico* physiologically based kinetic modeling. *Arch. Toxicol.* 2015, *89*, 1135–1148.
- [45] Strikwold, M., Spenkink, B., Woutersen, R., Rietjens, I. C. M. et al., Combining *in vitro* embryotoxicity data with physiologically based kinetic (PBK) modelling to define *in vivo* dose–response curves for developmental toxicity of phenol in rat and human. *Arch. Toxicol.* 2013, *87*, 1709–1723.
- [46] Gimenez-Bastida, J. A., Gonzalez-Sarrias, A., Vallejo, F., Espin, J. C. et al., Hesperetin and its sulfate and glucuronide metabolites inhibit TNF- $\alpha$  induced human aortic endothelial cell migration and decrease plasminogen activator inhibitor-1 (PAI-1) levels. *Food Funct.* 2016, *7*, 118–126.
- [47] Kortenkamp, A., Backhaus, T., Faust, M., State of the art on mixture toxicity. Report. 2009. Available from: [http://ec.europa.eu/environment/chemicals/effects/pdf/report\\_mixture\\_toxicity.pdf](http://ec.europa.eu/environment/chemicals/effects/pdf/report_mixture_toxicity.pdf).
- [48] Khan, M. K., Rakotomanomana, N., Dufour, C., Dangles, O., Binding of citrus flavanones and their glucuronides and chalcones to human serum albumin. *Food Funct.* 2011, *2*, 617–626.
- [49] Güllden, M., Seibert, H., *In vitro–in vivo* extrapolation: estimation of human serum concentrations of chemicals equivalent to cytotoxic concentrations *in vitro*. *Toxicology* 2003, *189*, 211–222.
- [50] Güllden, M., Mörchel, S., Tahan, S., Seibert, H., Impact of protein binding on the availability and cytotoxic potency of organochlorine pesticides and chlorophenols *in vitro*. *Toxicology* 2002, *175*, 201–213.
- [51] Xie, M.-X., Xu, X.-Y., Wang, Y.-D., Interaction between hesperetin and human serum albumin revealed by spectroscopic methods. *Biochim. Biophys. Acta.* 2005, *1724*, 215–224.
- [52] Mahesha, H. G., Singh, S. A., Srinivasan, N., Rao, A. G. A., A spectroscopic study of the interaction of isoflavones with human serum albumin. *FEBS J.* 2006, *273*, 451–467.
- [53] EFSA, Guidance of the Scientific Committee on a request from EFSA on the use of the benchmark dose approach in risk assessment. *EFSA J.* 2009, *1150*, 1–72.
- [54] Morand, C., Dubray, C., Milenkovic, D., Lioger, D. et al., Hesperidin contributes to the vascular protective effects of orange juice: a randomized crossover study in healthy volunteers. *Am. J. Clin. Nutr.* 2011, *93*, 73–80.
- [55] Milenkovic, D., Deval, C., Dubray, C., Mazur, A. et al., Hesperidin displays relevant role in the nutrigenomic effect of orange juice on blood leukocytes in human volunteers: a randomized controlled cross-over study. *PLoS One* 2011, *6*, e26669.
- [56] Sánchez-Moreno, C., Cano, M. P., de Ancos, B., Plaza, L. et al., High-pressurized orange juice consumption affects plasma vitamin C, antioxidative status and inflammatory markers in healthy humans. *J. Nutr.* 2003, *133*, 2204–2209.
- [57] Argikar, U. A., Unusual glucuronides. *Drug. Metab. Dispos.* 2012, *40*, 1239–1251.
- [58] Boersma, M. G., van der Woude, H., Bogaards, J., Boeren, S. et al., Regioselectivity of phase II metabolism of luteolin and quercetin by UDP-glucuronosyl transferases. *Chem. Res. Toxicol.* 2002, *15*, 662–670.
- [59] Matsumoto, H., Ikoma, Y., Sugiura, M., Yano, M. et al., Identification and quantification of the conjugated metabolites derived from orally administered hesperidin in rat plasma. *J. Agric. Food Chem.* 2004, *52*, 6653–6659.